Tunable titanium metal-organic frameworks with infinite Ti-O rod for highly efficient visible-light-driven photocatalytic H_2 evolution

Changqing Li,[a]‡ Hui Xu,[b]‡ Junkuo Gao,[a,c*] Wenna Du,[d] Liqing Shangguan,[a] Xin Zhang,[c] Rui-Biao Lin,[c] Hui Wu,[e] Wei Zhou,[e] Xinfeng Liu,[d*] Juming Yao,[a] Banglin Chen[c*]

[a]Institute of Fiber based New Energy Materials, The Key Laboratory of Advanced Textile Materials and Manufacturing Technology of Ministry of Education, College of Materials and Textiles, Zhejiang Sci-Tech University, Hangzhou 310018, P. R. China

[b]College of Materials Science and Engineering, China Jiliang University, Hangzhou 310018, PR China

[c]Department of Chemistry, University of Texas at San Antonio, One UTSA Circle, San Antonio, Texas 78249-0698, United States

[d]Division of Nanophotonics, CAS Key Laboratory of Standardization and Measurement for Nanotechnology, CAS Center for Excellence in Nanoscience, National Center for Nanoscience and Technology, Beijing 100190, China

[e]NIST Center for Neutron Research, National Institute of Standards and Technology, Gaithersburg, Maryland 20899-6102, United States

1. Experimental Details

Experimental Section

Materials. All chemicals were purchased from Alfa Aesar, TCI chemical and Aldrich and used without further purification. Extra dry DMF packaged with molecular sieves was obtained from Alfa Aesar. Organic ligands H_3TCA[1], H_3BTB[2] and H_3BTCA[3] were synthesized according to literatures.

Characterization.

Powder X-ray diffraction data (XRD) were recorded on a Bruker D8 Advance diffractometer with a graphite-monochromatized Cu *Ka* radiation. FTIR spectra were recorded from KBr pellets by using a Perkin Elmer FTIR SpectrumGX spectrometer. Thermogravimetric analysis (TGA) was carried out on a TA Instrument Q500 Thermogravimetric Analyzer at a heating rate of 10 ^oC/min

up to 1000 °C under N_2 atmosphere and air atmosphere. UV-Vis absorption spectra were obtained using a Shimadzu UV-2450 spectrophotometer. The optical diffuse reflectance spectra were measured on a Hitachi UH-4150 UV-vis spectrometer equipped with an integrating sphere. $BaSO_4$ was used as the reference material, and the polycrystalline samples were ground well before the measurement. The absorption (α/S) data were calculated from the reflectance using the Kubelka–Munk function: $\alpha/S = (1-R)^2/2R$, in which R is the reflectance at a given wavelength, α is the absorption coefficient, and S is the scattering coefficient. X-ray photoelectron spectroscopy (XPS) data were obtained with a Thermal Fisher Scientific K-Alpha electron spectrometer. field Emission scanning electron microscope (SEM) image were obtained by Carl Zeiss Vltra55 microscope and transmission electron microscopy (TEM) image were obtained by JEM-2100. The specific surface areas of all samples were measured by the Brunauer-Emmett-Teller (BET) method. The N_2 adsorption-desorption isotherms at 77 K were measured on a Micrometrics ASAP 2020 system to evaluate their pore structures. All the samples were degassed at 160 °C for 2 hours before the surface area measurements. Simulation of the XRD pattern was carried out by the crystal data and diffraction-crystal module of the Mercury (Hg) program version 3.1 available free of charge via the Internet http://www.ccdc.cam.ac.uk.

Synthesis of ZSTU-1

4,4',4''-nitrilotribenzoicacid (H_3TCA) (377 mg, 1 mmol) was added to 5 mL of extra dry DMF in a 25 mL Teflon-lined stainless-steel autoclave. After ultrasound for 1 h to obtain clear solution, titanium isopropoxide (0.31 mL, 1 mmol) was added dropwise with stirring and a bright yellow slurry formed. The mixture was heated at 180 °C for 24 h in an oven. Then, the mixture was naturally cooled to room temperature and washed with DMF and methanol three times each. Bright yellow crystalline powder was obtained. Yield: 40 % (based on Ti).

Synthesis of ZSTU-2

1,3,5-Tri (4-carboxyphenyl) benzene (H_3BTB) (500 mg, 1.14 mmol) was added to 5 mL of extra dry DMF in a 25 mL Teflon-lined stainless-steel autoclave. After ultrasound for 1 h to obtain clear solution, titanium isopropoxide (0.2 mL, 0.64 mmol) was added dropwise with stirring and a white slurry formed. The mixture was heated at 180 °C for 30 h in an oven. Then, the mixture was naturally cooled to room temperature and washed with DMF and methanol three times each. White crystalline powder was obtained. Yield: 30 % (based on Ti). For activation of **ZSTU-2**, the powders were

heated with DMF at 120 °C for eight hours to remove any organic ligands, and reflux with methanol at 80 °C for eight hours to remove DMF, then dried in a vacuum oven at 60 °C for 12 hours.

Synthesis of ZSTU-3

4',4''',4''''-nitrilotris(([1,1'-biphenyl]-4-carboxylicacid)) (H_3BTCA) (400 mg, 0.66 mmol) was added to 5 mL of extra dry DMF in a 25 mL Teflon-lined stainless-steel autoclave. After ultrasound for 1 h to obtain clear solution, titanium isopropoxide (0.16 mL, 0.5 mmol) was added dropwise with stirring and a yellow slurry formed. The mixture was heated at 180 °C for 30 h in an oven. Then, the mixture was naturally cooled to room temperature and washed with DMF and methanol three times each. Yellow powder was obtained. Yield: 30 % (based on Ti). For activation of **ZSTU-3**, the powders were heated with DMF at 120 °C for eight hours to remove any organic ligands, and reflux with methanol at 80 °C for eight hours to remove DMF, then dried in a vacuum oven at 60 °C for 12 hours.

Electrode preparation. To prepare the photoelectrodes, 10 mg of **ZSTU-1** was first ground using a marble mortar and pestle, and then added into 1 mL of 98% ethanol (Merck). The as-prepared solution was placed on a 60˚C hotplate stirrer overnight to ensure that the **ZSTU-1** was completely dissolved in the solution. Meanwhile, the fluorine-doped tin oxide (F:SnO_2, Tec 15, 10Ω/□, Hartford Glass Company) were cleaned thoroughly by sonication in 5% detergent for 30 min first and then rinsed with de-ionized water (DI water) for several times, which were followed by sonication in DI water for 15 min. The sonication in DI water process was repeated for three times. Before coating with **ZSTU-1**, the FTO substrates were cleaned with UV-ozone plasma for 15 min to remove the organic residues. After that, 10 µl of the 10 mg/ml **ZSTU-1** solution was dropped onto the surface of FTO substrate, which was masked by a 3M scotch tape with an exposed area of 1.0 × 1.0 cm^2, and then dried in air at 60˚C on a hotplate. This step was repeated four times to achieve a uniform coverage of **ZSTU-1** on FTO. Electrode preparation of **ZSTU-2** and **ZSTU-3** is the same as the **ZSTU-1**.

Photoelectrochemical measurements. The photoelectrochemical tests were performed using an electrochemical workstation (Zahner Zennium). A three-electrode set-up, with a platinum plate (1 × 2 cm^2) and an Ag/AgCl electrode as the counter and reference electrodes, respectively, was used to study the photovoltage response (illuminated open circuit potential). Meanwhile, the photocurrent test was carried out using a two-electrode set-up, in which the working electrode (**ZSTU-1**/FTO)

and the counter electrode (Pt) were short-circuited. 0.5 M Na_2SO_4 solution (pH = 7.0) was used as the electrolyte throughout the photoelectrochemical tests. Prior to each measurement, the electrolyte was deaerated by purging it with argon continuously for 30 minutes. A 150 W tungsten halogen lamp (Filtered, λ > 400nm) was used as the visible light source, and the illumination intensity on the surface of the electrode was approximately 100 mW/cm^2.

Photocatalytic experiments. The evaluation of photocatalytic activities of the samples for the visible light photocatalytic hydrogen production was performed in a 160 mL optical reaction vessel under condensing circulating water (1℃). First, co-catalyst platinum was plated on the catalyst by thermal reduction of glucose in 80℃ methanol maintaining 3 hours, then the sample was centrifuged and dried in a vacuum oven at 60℃. The procedure was as follows: 50 mg of sample was dispersed into acetonitrile, triethanolamine and H_2O mixed system [102 mL, V(MeCH): V(TEOA):V(H_2O) = 9:1:0.2] by using TEOA as a sacrificial reagent. A 300W Xenon arc lamp coupled with a UV cut-off filter (λ > 420 nm) was used as the light source. The suspension is vacuumed to ensure that the system reaches an anaerobic environment. Hydrogen gas was detected by on-line gas chromatography (Techcomp-GC7900, argon as a carrier gas) with a thermal conductivity detector.

Transient absorption. Femtosecond transient absorption spectra (fs-TAS) measurements were performed by using a commercial fs-TAS system, specifically, HELIOS (Ultrafast Systems). The 800 nm pulses from a Coherent Astrella regenerative amplifier (80 fs, 1 kHz, 2.5μJ per pulse), seeded by a Coherent Vitara-s oscillator (35 fs, 80 MHz), was used to pump an optical parametric amplifier (Coherent, OperA Solo) to generate excitation pulse at 380 nm. The pump beam was chopped at 500 Hz with pump fluence at ~5 μJ cm−2, while a small fraction of the 800 nm output from the Astrella was fed to a sapphire crystal in the HELIOS for generating the WLC. A 750 nm SPF was placed in the probe path before the sample to filter out the residual 800 nm in the WLC. The system has an ultimate temporal resolution of ~130 fs.

Density-functional theory calculations. Our First-principles density-functional theory (DFT) calculations were performed using the Quantum-Espresso package.[4] A semi-empirical addition of dispersive forces to conventional DFT.[5] We used Vanderbilt-type ultrasoft pseudopotentials and the generalized gradient approximation (GGA) with the Perdew-Burke-Ernzerhof (PBE) exchange

correlation. A cutoff energy of 544 eV and a 1×1×2 *k*-point mesh (generated using the Monkhosrt-Pack scheme) were found to be enough for total energy to converge within 0.01 meV/atom. The structure models of Ti-MOFs were fully optimized with respect to atomic coordinates.

2. Structural information.

Table S1. Atomic coordinates and refined unit cell parameters of **ZSTU-1**.

Name	**ZSTU-1**		
Space group	P63/MCM		
a (Å)	17.274(2)		
c (Å)	11.805(2)		
Unit Cell Volume (Å^3)	3057.6(8)		
Atom name	x	y	z
C1	0.52699	0.31724	0.43219
C2	0.43445	0.27058	0.43205
C3	0.57298	0.28649	0.5
C4	0.38841	0.19421	0.5
C5	0.28976	0.14488	0.5
H1	0.56492	0.37702	0.38034
H2	0.39595	0.29118	0.37929
H3	0.20151	0.0648	0.25
N1	0.66667	0.33333	0.5
O1	0.2512	0.17013	0.4298
O2	0.16725	0.09527	0.25
O3	0.09921	0.09921	0.57296
Ti1	0.11677	0.11677	0.39406

Table S2. Atomic coordinates and refined unit cell parameters of **ZSTU-2**.

Name	**ZSTU-2**		
Space group	P63/MCM		
a (Å)	20.1600		
c (Å)	11.7580		
Unit Cell Volume (Å^3)	4138.52		
Atom name	x	y	z
C1	0.45935	0.27628	0.43504
C2	0.37962	0.23613	0.43415
C3	0.50071	0.25036	0.5

C4	0.33894	0.16947	0.5
C5	0.25324	0.12662	0.5
C6	0.58557	0.29278	0.5
C7	0.62667	0.37333	0.5
H1	0.49067	0.32762	0.38279
H2	0.34745	0.25529	0.38233
H3	0.17401	0.05689	0.25
H4	0.59539	0.40461	0.5
O1	0.21902	0.14791	0.43062
O2	0.14373	0.08207	0.25
O3	0.0846	0.0846	0.57297
Ti1	0.10312	0.10312	0.39513

Table S3. Atomic coordinates and refined unit cell parameters of **ZSTU-3**.

Name	**ZSTU-3**		
Space group	P63/MCM		
a (Å)	24.6300		
c (Å)	11.7580		
Unit Cell Volume (Å^3)	6177.22		
Atom name	x	y	z
C1	0.36837	0.20933	0.41111
C2	0.30354	0.17766	0.41169
C3	0.56832	0.32392	0.43856
C4	0.50354	0.29182	0.44037
C5	0.60101	0.30051	0.5
C6	0.46996	0.23498	0.5
C7	0.4016	0.2008	0.5
C8	0.27136	0.13568	0.5
C9	0.20239	0.1012	0.5
H1	0.39383	0.24024	0.34038
H2	0.27657	0.18377	0.34448
H3	0.59436	0.36777	0.39164
H4	0.47845	0.31137	0.3955
H5	0.14111	0.04526	0.25
N1	0.66667	0.33333	0.5
O1	0.17541	0.11841	0.42872
O2	0.1168	0.06633	0.25
O3	0.06949	0.06949	0.57286
Ti1	0.08167	0.08167	0.39379

3. Figures

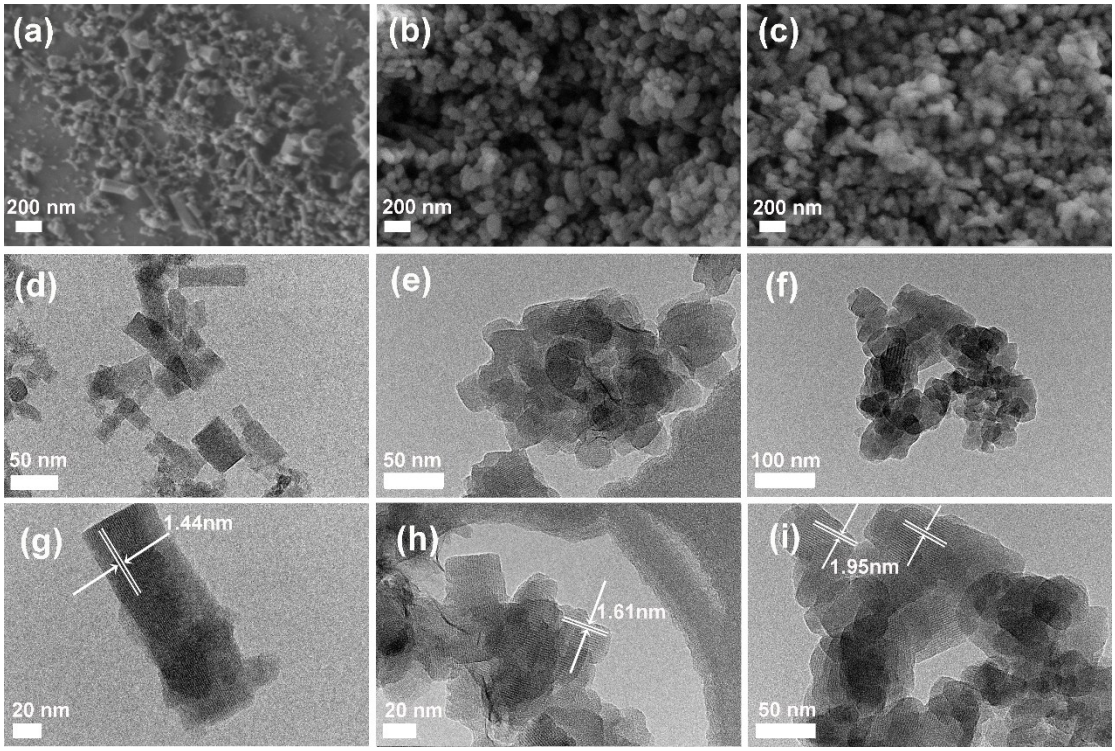

Figure S1. SEM of **ZSTU-1** (a), **ZSTU-2** (b) and **ZSTU-3** (c). TEM of **ZSTU-1** (d) (g), **ZSTU-2** (e) (h) and **ZSTU-3** (f) (i).

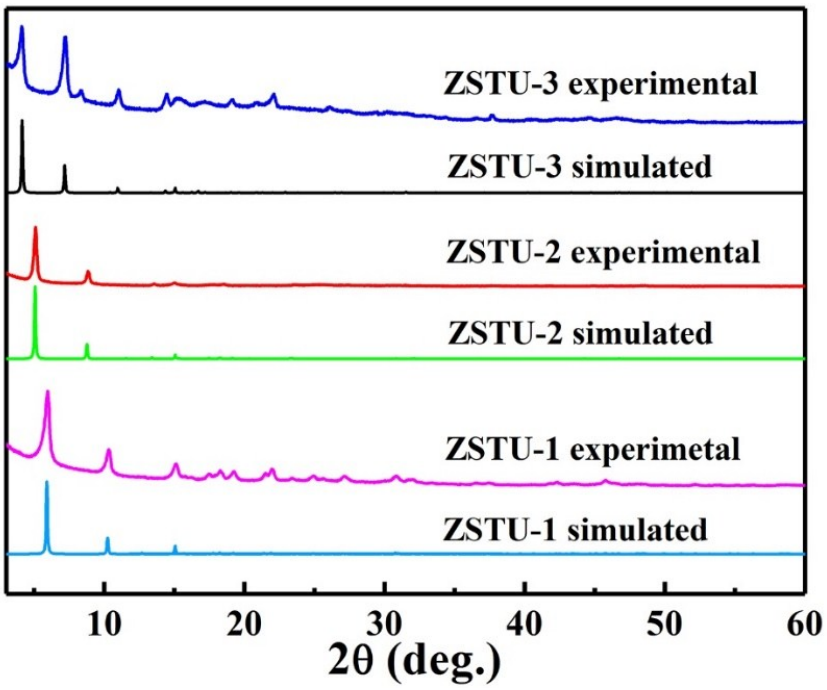

Figure S2. The experimental and simulated powder XRD patterns of **ZSTU-1**, **ZSTU-2** and **ZSTU-3**.

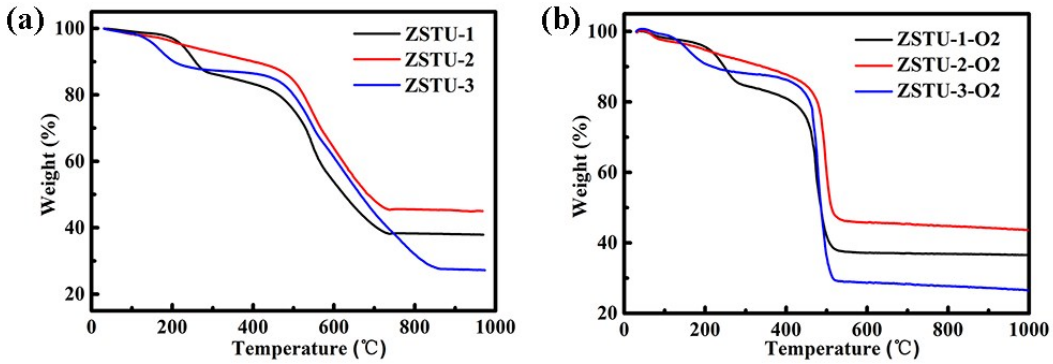

Figure S3. The TG curves of MOF **ZSTU-1**, **ZSTU-2** and **ZSTU-3** under N_2 atmosphere and air atmosphere.

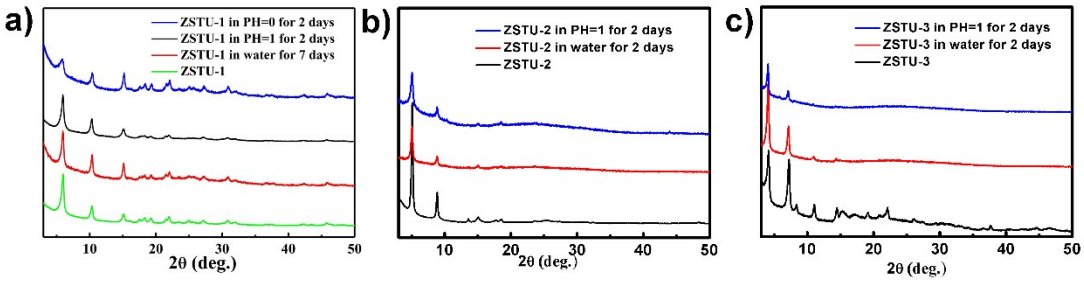

Figure S4. Powder XRD pattern of **ZSTU-1 (a), ZSTU-2 (b)** and **ZSTU-3 (c)** at different environments.

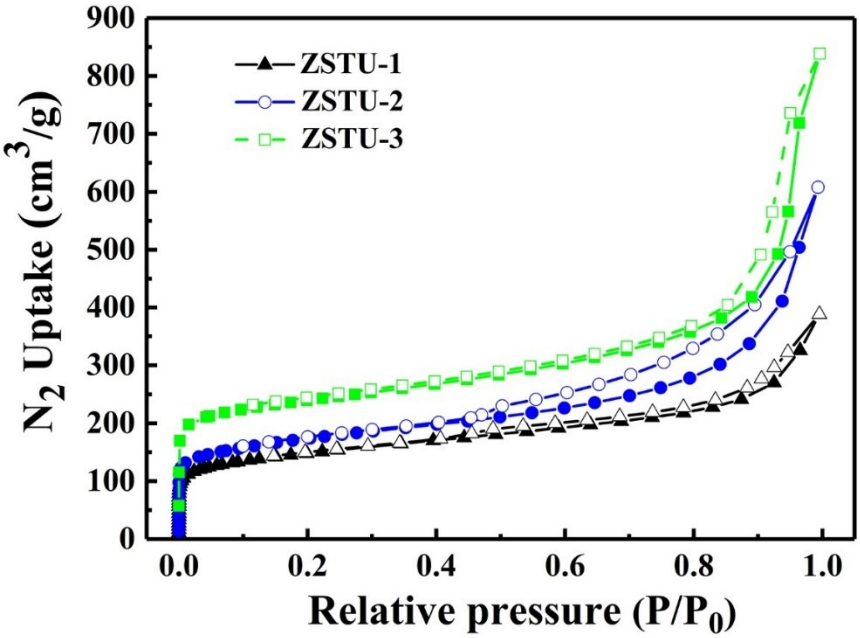

Figure S5. The N_2 adsorption isotherm of **ZSTU-1**, **ZSTU-2** and **ZSTU-3** at 77 K.

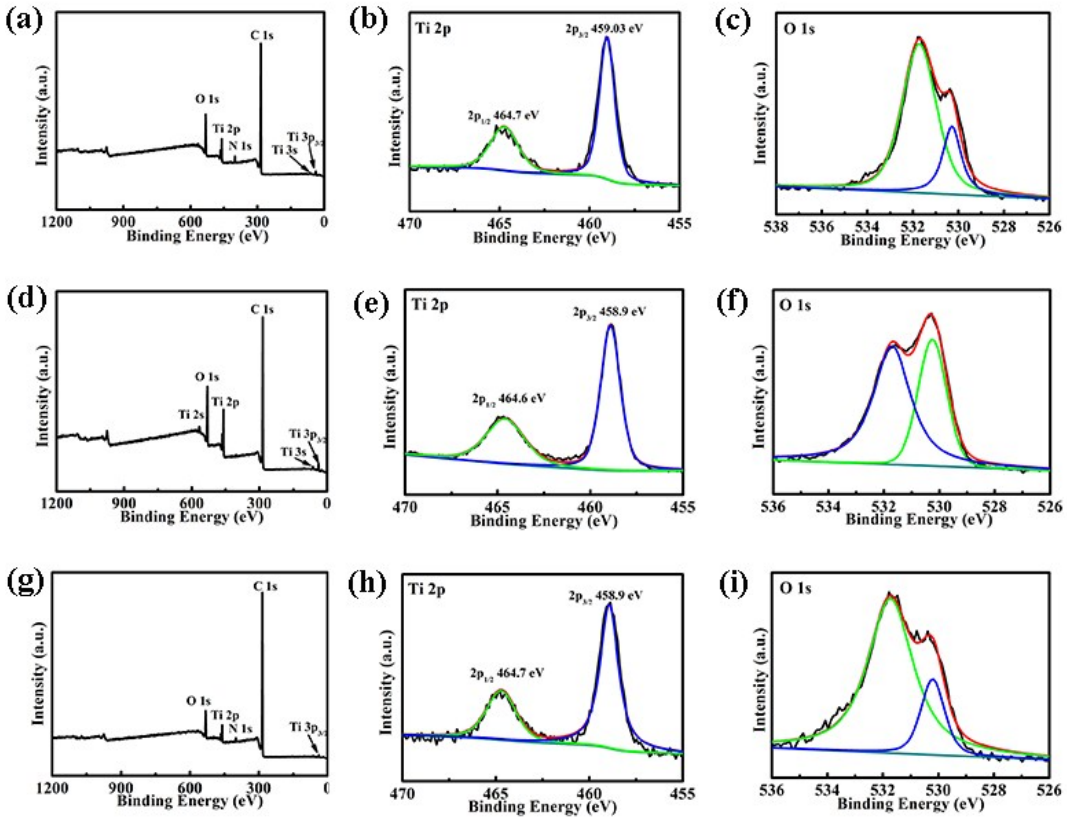

Figure S6. XPS pattern of **ZSTU-1** (a) (b) (c)， **ZSTU-2** (d) (e) (f) and **ZSTU-3** (g) (h) (i).

The XPS survey scan spectrum indicates that **ZSTU-1** (a) and **ZSTU-3** (g) including C, N, O and Ti elements, then **ZSTU-2** (d) consists of C, O and Ti elements. About Ti element, though Figure S6 (b), (e), (h), there are two peaks located at around 464 eV and 459 eV, corresponding to Ti $2p_{1/2}$ and Ti $2p_{3/2}$, respectively, suggesting a normal state of Ti^{4+}. In the high-resolution O 1s spectrum (c), (f), (i), there is a clear peak at 530.2 eV can be assigned to Ti–O–Ti, and another strong peak could be observed at 531.6 eV, corresponds to the surface hydroxyl species.

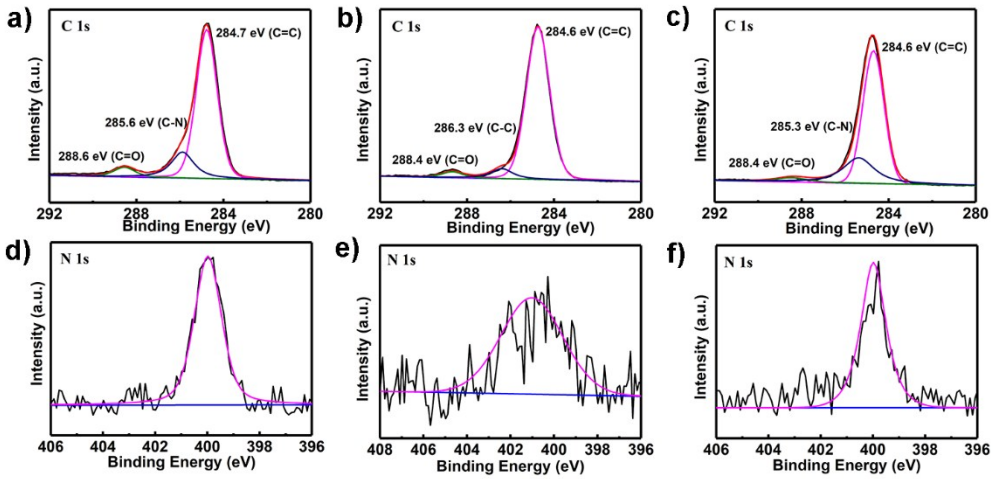

Figure S7. XPS pattern of **ZSTU-1** (a) (d)，**ZSTU-2** (b) (e) and **ZSTU-3** (c) (f).

The XPS spectrum of the ZSTU-1 (a) and ZSTU-3 (c) in the C 1s region shows three peaks at about 284.6, 285.6 and 288.4 eV, can be assigined to C=C, C-N and C=O, respectively. Then for ZSTU-2 (b), three peaks centering at 284.5, 286.3, and 288.5 eV can be assigned to C=C, C-C and C=O, respectively. About N element, though Figure S6-2 (d) and (f), ZSTU-1 and ZSTU-3 show a clear peak at 399.6 eV can be assigned to N-$(C)_3$. For ZSTU-2 (e), BTB without nitrogen, so there is a weak peak mainly caused by DMF.

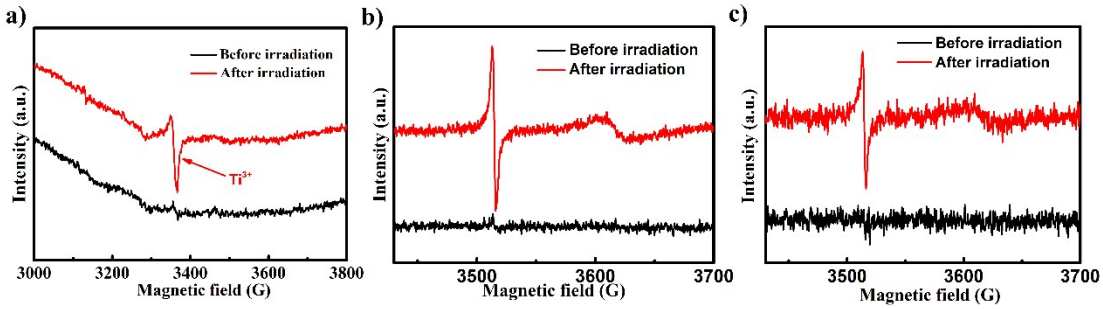

Figure S8. EPR spectra observed at 77 K for **ZSTU-1** (a), **ZSTU-2** (b) **and ZSTU-3** (c) immersed in CH_3CN/TEOA/H_2O (9:1:0.2) solution before and after visible-light irradiation ($\lambda > 420$ nm).

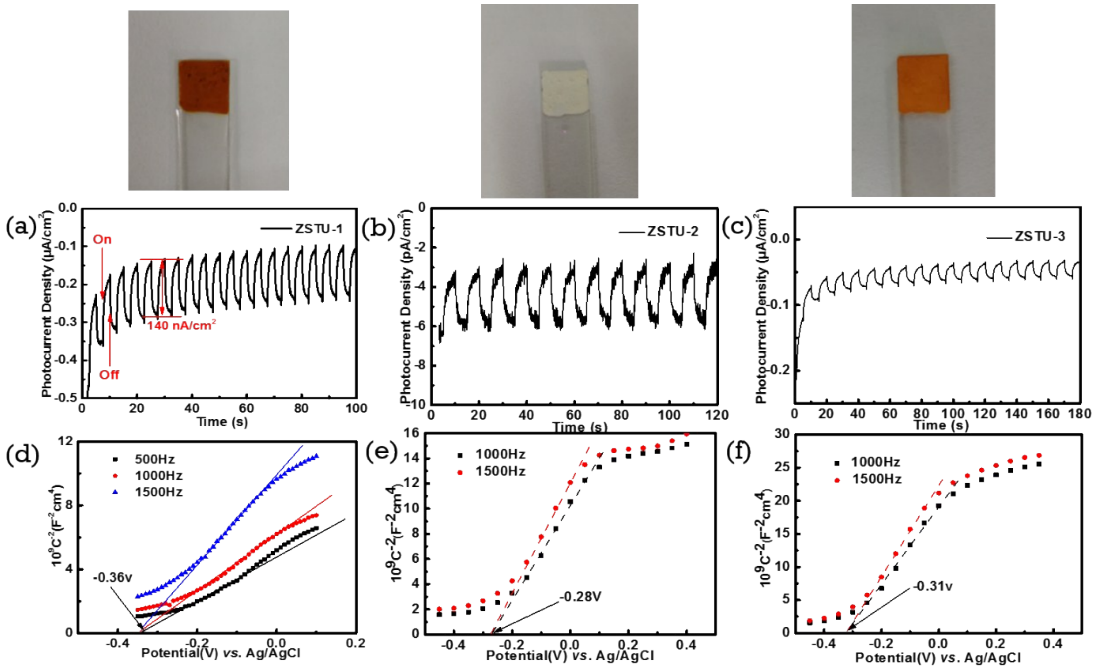

Figure S9. Transient photocurrent responses of **ZSTU-1** (a), **ZSTU-2** (b) and **ZSTU-3**(c), Mott–Schottky plot of the **ZSTU-1** (d), **ZSTU-2** (e) and **ZSTU-3** (f) in 0.5 M Na_2SO_4 solution measured at different frequency of 500, 1000 and 1500 Hz. The flat-band potential of the three samples are indicated by the intercept of the dashed lines.

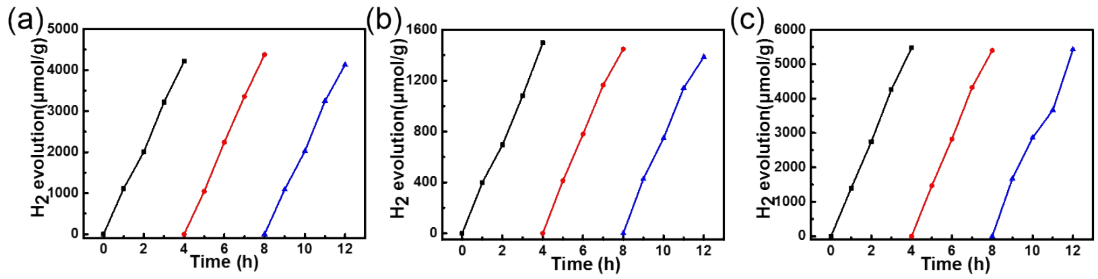

Figure S10. The Hydrogen production cycle of **ZSTU-1**, **ZSTU-2** and **ZSTU-3**.

Table S4. A detailed comparison of hydrogen production performance between titanium-based MOFs and other typical photocatalytic MOFs.

photocatalyst	Incident light	Reactant solution	H_2 evolution rate (umol h^{-1} g^{-1})	Ref.
ZSTU-1	300 W Xe-lamp $\lambda \geq 420$ nm	TEOA/MeCN/H_2O	1095	This work
ZSTU-2	300 W Xe-lamp	TEOA/MeCN/H_2O	374	This work

ZSTU-3	$\lambda \geq 420$ nm 300 W Xe-lamp	TEOA/MeCN/H_2O	1368	This work
PCN-416	$\lambda \geq 420$ nm 300 W Xe-lamp	TEOA/MeCN/H_2O	484	[6]
PCN-415-NH_2	$\lambda \geq 380$ nm 300 W Xe-lamp	TEOA/MeCN/H_2O	594	[6]
Pt/NH2-MIL-125	$\lambda \geq 380$ nm 300 W Xe-lamp $\lambda \geq 420$ nm	TEOA/MeCN	588	[7]
C_3N_4/MIL-125-NH_2	300 W Xe-lamp 320 nm $\leq \lambda \leq$ 780nm	H_2O/TEOA	1123	[8]
Pt@UiO-66-NH2	300 W Xe-lamp	TEOA/MeCN/H_2O	257	[7]
Ti-MOF-Ru(tpy)$_2$	$\lambda \geq 380$ nm 300 W Xe-lamp	H_2O/TEOA	181	[9]
Al-PMOF	$\lambda \geq 420$ nm 300 W Xe-lamp	H_2O/TEOA	200	[10]
MIL-100 (Fe)	$\lambda \geq 420$ nm 300 W Xe-lamp	H_2O/MeOH	109	[11]
MOF-253 (Al)	$\lambda \geq 420$ nm 300 W Xe-lamp	H_2O/TEOA	100	[12]
HM-TiPPh	$\lambda \geq 420$ nm 300 W Xe-lamp	H_2O/TEOA	945	[13]
MUV-10 (Ti-Mn)	$\lambda \geq 400$ nm 300 W Xe-lamp	H_2O/MeOH	270	[14]
	$\lambda \geq 420$ nm			

References

[1] Q. Yao, A. Bermejo Gómez, J. Su, V. Pascanu, Y. Yun, H. Zheng, H. Chen, L. Liu, H. N. Abdelhamid, B. n. Martín-Matute, *Chem. Mater.* **2015**, *27*, 5332-5339.

[2] J. Park, D. Feng, H.-C. Zhou, *J. Am. Chem. Soc.* **2015**, *137*, 1663-1672.

[3] Y.-P. He, Y.-X. Tan, J. Zhang, *Cryst. Growth Des.* **2012**, *13*, 6-9.

[4] P. Giannozzi, S. Baroni, N. Bonini, M. Calandra, R. Car, C. Cavazzoni, D. Ceresoli, G. L. Chiarotti, M. Cococcioni, I. Dabo, *J. Phys.: Condens. Matter* **2009**, *21*, 395502.

[5] V. Barone, M. Casarin, D. Forrer, M. Pavone, M. Sambi, A. Vittadini, *J. Comput. Chem.* **2009**, *30*, 934-939.

[6] S. Yuan, J. S. Qin, H. Q. Xu, J. Su, D. Rossi, Y. P. Chen, L. L. Zhang, C. Lollar, Q. Wang, H. L. Jiang, D. H. Son, H. Y. Xu, Z. H. Huang, X. D. Zou, H. C. Zhou, *ACS Central Sci.* **2018**, *4*, 105-111.

[7] D. Sun, W. Liu, Y. Fu, Z. Fang, F. Sun, X. Fu, Y. Zhang, Z. Li, *Chem. Eur. J.* **2014**, *20*, 4780-4788.

[8] G. Zhou, M.-F. Wu, Q.-J. Xing, F. Li, H. Liu, X.-B. Luo, J.-P. Zou, J.-M. Luo, A.-Q. Zhang, *Appl. Catal. B: Environ.* **2018**, *220*, 607-614.

[9] T. Toyao, M. Saito, S. Dohshi, K. Mochizuki, M. Iwata, H. Higashimura, Y. Horiuchi, M. Matsuoka, *Chem. Commun.* **2014**, *50*, 6779-6781.

[10] A. Fateeva, P. A. Chater, C. P. Ireland, A. A. Tahir, Y. Z. Khimyak, P. V. Wiper, J. R. Darwent, M. J. Rosseinsky, *Angew. Chem. Int. Ed.* **2012**, *51*, 7440-7444.

[11] D. Wang, Y. Song, J. Cai, L. Wu, Z. Li, *New J. Chem.* **2016**, *40*, 9170-9175.

[12] T. Zhou, Y. Du, A. Borgna, J. Hong, Y. Wang, J. Han, W. Zhang, R. Xu, *Energy Environ. Sci.* **2013**, *6*, 3229-3234.

[13] H. Li, Y. Sun, Z. Y. Yuan, Y. P. Zhu, T. Y. Ma, *Angew. Chem. Int. Ed.* **2018**, *57*, 3222-3227.

[14] J. Castells-Gil, N. M. Padial, N. Almora-Barrios, J. Albero, A. R. Ruiz-Salvador, J. González-Platas, H. García, C. Martí-Gastaldo, *Angew. Chem. Int. Ed.* **2018**, *57*, 8453-8457.